· Article · **Advances in Polar Science**
doi: 10.12429/j.advps.2024.0042 June 2025 Vol. 36 No. 2: 95-112

Geomorphometry of the Bunger Hills, East Antarctica

Igor FLORINSKY[1*] & Sofya ZHARNOVA[2]

[1] Institute of Mathematical Problems of Biology, Keldysh Institute of Applied Mathematics, Russian Academy of Sciences, Pushchino 142290, Russia;
[2] National Research Tomsk State University, Tomsk 634050, Russia

Received 18 December 2024; accepted 1 April 2025; published online 30 June 2025

Abstract Geomorphometric modeling and mapping of Antarctic oases are promising for obtaining new quantitative knowledge about the topography of these unique landscapes and for the further use of morphometric information in Antarctic research. Within the framework of a project to create a thematic physical-geographical scientific reference geomorphometric atlas of ice-free areas of Antarctica, we performed geomorphometric modeling and mapping of the Bunger Hills (Knox Coast, Wilkes Land, East Antarctica), one of the largest Antarctic oases. By processing a fragment of the Reference Elevation Model of Antarctica (REMA) covering the Bunger Hills and adjacent glaciers, we created, for the first time, a series of 37 medium- to large-scale maps of nine of the most scientifically important morphometric variables (i.e., slope gradient, slope aspect, vertical curvature, horizontal curvature, maximal curvature, minimal curvature, catchment area, topographic wetness index, and stream power index). The morphometric maps describe the topography of the Bunger Hills in a quantitative, rigorous, and reproducible manner. New morphometric data can be useful for further geological, geomorphological, glaciological, ecological, and hydrological studies of this Antarctic oasis.

Keywords **digital terrain modeling, digital elevation model (DEM), topography, geomorphometry, mapping, Antarctica**

Citation: Florinsky I, Zharnova S. Geomorphometry of the Bunger Hills, East Antarctica. Adv Polar Sci, 2025, 36(2): 95-112, doi: 10.12429/j.advps.2024.0042

1 Introduction

Antarctic oases are ice-free coastal, near-shelf glacier, and mountainous areas of Antarctica (Alexandrov, 1985; Bardin, 1970; Bölter et al., 2002; Korotkevich, 1972; Markov et al., 1970; Pickard, 1986; Simonov, 1971; Sokratova, 2010). Landscapes of Antarctic oases are characterized by the presence of stream and lake systems in the summer; some lakes do not freeze even in winter. The presence of primitive soils (Bockheim, 2015), mosses (Ochyra et al., 2008), and lichens (Øvstedal and Lewis Smith, 2001) is also typical of Antarctic oases.

Topography is a key component of the environment. Being a result of the interaction of endo- and exogenous processes of various scales and reflecting the geological structure, topography determines prerequisites for the gravity-driven migration and accumulation of moisture and other substances along the land surface and in the near-surface layer, controls thermal, hydrological, and wind regimes of the terrain, distribution of soil and vegetation cover, etc.

The rigor and reproducibility of topographic studies are ensured by geomorphometry, a discipline with a developed physical and mathematical theory and a powerful apparatus of computational methods, the subject of which is the modeling and analysis of topography as well as relationships between topography and other components of geosystems (Florinsky, 2017, 2025a; Hengl and Reuter, 2009; Lv et al., 2017; Minár et al., 2016; Moore et al., 1991;

* Corresponding author. ORCID: 0000-0003-1273-5912. E-mail: iflor@mail.ru

Shary et al., 2002; Wilson and Gallant, 2000).

Geomorphometric modeling and mapping of Antarctic oases (Florinsky, 2023a, 2023b, 2025b) are promising for obtaining new quantitative knowledge about the topography of these terrains and for the further use of morphometric information in solving problems of geomorphology, geology, glaciology, soil science, ecology, and other geosciences.

A project has recently been launched to create a thematic physical-geographical scientific reference geomorphometric atlas of ice-free areas of Antarctica (Florinsky, 2024, 2025b). As part of this project, we carried out a geomorphometric modeling and mapping of the Bunger Hills (Wilkes Land, East Antarctica), one of the largest Antarctic oases. We created a set of medium- to large-scale morphometric maps of this territory, which quantitatively, rigorously, and reproducibly describe the topography of the oasis. The results are presented in this article.

2 Study area

The Bunger Hills are located in the northwest of the Knox Coast, Wilkes Land, between 66°S–66.4°S, and 100.4°E–101.4°E, about 25 km north of the Antarctic Circle. The oasis was discovered in January 1947 by members of the U.S. Navy's Antarctic Operation Highjump. It was named after the pilot David Bunger, who was conducting an aerial survey of the coast and landed his seaplane on one of the marine inlets within the oasis (Byrd, 1947).

The Bunger Hills (Figure 1) are one of the largest Antarctic ice-free areas. Its size is approximately 20 km by 40 km, including both land and marine inlets. The total area of its land mass is about 450 km^2.

The oasis is surrounded by glaciers on all sides. To the east it is bounded by the Remenchus outlet glacier and a margin of the Antarctic Ice Sheet, to the south by the Apfel outlet glacier, to the west by the Edisto outlet glacier, and to the north by the Shackleton Ice Shelf.

Marine inlets (e.g., Edisto Channel, Cacapon Inlet, and some minor bays) naturally divide the oasis into two main parts (Bolshiyanov, 1990; Gibson, 2006; Grigoriev, 1962; Simonov, 1971; Wisniewski, 1983):

1) The southern land mass with an area of about 280 km^2, including the Fuller (Kashalot) Island.

2) Several large, near-east-west stretching peninsulas and islands with the total area of about 170 km^2 in the north of the oasis, such as the Booth (Charnockite) and Geomorfologov peninsulas as well as the Thomas and Currituck (Geografov) islands.

To the north of the Bunger Hills lies the Highjump Archipelago, consisting of small islands and nunataks. Within the study area, three hypsometric levels can be distinguished (Figure 1):

1) The Antarctic Ice Sheet, bordering the Bunger Hills to the east, has maximum elevations of about 690–700 m above sea level.

2) The Bunger Hills, where the elevations are mostly in the range of 100–120 m, with maxima of around 160–170 m above sea level.

3) Outlet and shelf glaciers characterized by lower elevations.

According to the physical-geographical zoning of Antarctic polar deserts (Korotkevich, 1972), the Bunger Hills belong to the Wilkes Land polar desert province. This province extends along the coast from 80°E to 160°E. It is characterized by the most severe climatic conditions: Throughout the year, constant katabatic winds prevail, which merge with cyclones during periods of their activity; average annual wind speeds are about 10–15 $m{\cdot}s^{-1}$, reaching 20 $m{\cdot}s^{-1}$ at the foot of the ice sheet (Korotkevich, 1972).

The Bunger Hills are composed of Precambrian, predominantly Lower Proterozoic rocks. These include gneisses, plagiogneisses, crystalline schists, and migmatites intruded by granitoids (charnockites) and cut by dolerite dykes (Markov et al., 1970; Ravich, 1957, 1960; Sheraton et al., 1995; Tucker et al., 2020).

The landscape of the oasis is a structural denudational hummocky terrain, which includes rocky hills and ridges separated by more or less closed tectonic depressions and hollows (Avsyuk et al., 1956; Bolshiyanov, 1990; Gibson, 2006; Grigoriev, 1962; Markov et al., 1970; Shumskiy, 1957; Simonov, 1971; Wisniewski, 1983).

Despite the low elevations (see above), the topography of the Bunger Hills is very contrasting because the landscape is dissected by numerous steep deep valleys located along fault lines (Bolshiyanov, 1990). Some valleys are filled with fresh flowing lakes and salty endorheic lakes. Fresh lakes are connected into a drainage system of the Algae River, the third longest river in Antarctica (Gibson et al., 2002).

There is evidence that the Bunger Hills were deglaciated between 30,000 and 10,000 years ago (Gore et al., 2001; Verkulich, 1995). The modern topography of the oasis was mainly formed in the pre-glacial era. Despite the repeated glaciation of the oasis, the glacial topography is not widespread. The exaration activity of glaciers was possibly expressed in the expansion of ancient valleys of structural denudational origin (Bolshiyanov, 1990).

The following landforms and geomorphic features are common in the Bunger Hills (Avsyuk et al., 1956; Grigoriev, 1962; Markov et al., 1970; Simonov, 1971):

1) Erosional and accumulative slope terraces, probably formed as a result of ancient glaciation processes.

2) Results of physical weathering, such as exfoliation joints, rock cracking, tafoni, wind furrows, and niches.

3) Cryogenic landforms dominated by patterned grounds, stone polygons, thermokarst depressions, ice-wedge polygons, and solifluction ground flows.

4) Ancient and modern glacial landforms, such as trough valleys, small tarns, and roches moutonnées. Ancient landforms are widespread, while modern ones are located at the edge of the ice sheet.

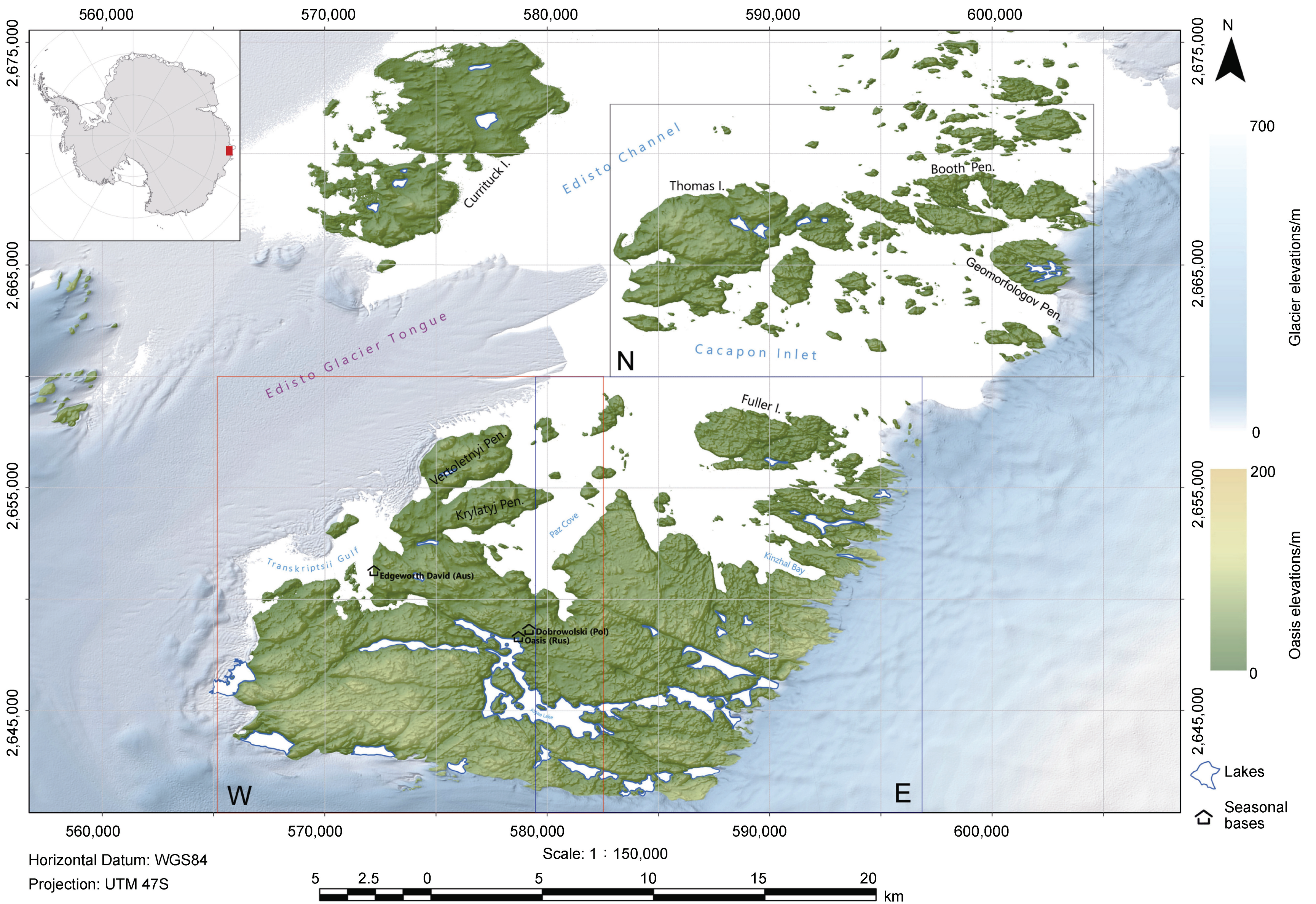

Figure 1 Bunger Hills: hypsometric map, scale 1 ∶ 150,000 and geographical location (insert map). Red frame (W) indicates the coverage of the 1 ∶ 75,000 scale maps for the western part of the southern Bunger Hills (see Figures 2a and 3a); blue frame (E) indicates the coverage of the 1 ∶ 75,000 scale maps for the eastern part of the southern Bunger Hills (see Figures 2b and 3b); black frame (N) indicates the coverage of the 1 ∶ 75,000 scale maps for the Booth (Charnockite) and Geomorfologov Peninsulas as well as Thomas Island (see Figures 4 and 5). Note: the maps for the western and eastern parts of the southern Bunger Hills overlap by 3 km in its central part.

There are three seasonal research bases in the Bunger Hills, such as Oasis (Russia), Dobrowolski (Poland), and Edgeworth David (Australia).

3 Materials and methods

As input data for geomorphometric modeling and mapping of the Bunger Hills, we used four digital elevation models (DEMs) with grid spacings of 2, 8, 10, and 32 m extracted from mosaics of the Reference Elevation Model of Antarctica (REMA) versions 1.1 and 2 (Howat et al., 2019, 2022). The REMA data were photogrammetrically constructed from hundreds of thousands of sub-meter resolution images of the WorldView-1, WorldView-2, and WorldView-3 spacecraft. REMA is the most complete and accurate DEM of Antarctica: its absolute errors do not exceed 1 m over most of the coverage area, while its relative errors are in the decimeter range (Polar Geospatial Center, 2023).

REMA is presented in the polar stereographic projection; elevations are given relative to the WGS84 ellipsoid. For the further study, all four extracted DEMs were reprojected into the UTM projection (zone 47S) while preserving the original grid spacings in interpolation. Each resulting DEM includes the Bunger Hills and adjacent glaciers, covering an area of 57.6 km by 37.4 km (Figure 1).

We carried out a comparative statistical and visual analysis of the four DEMs and found that, in terms of the level of data generalization, high-frequency noise suppression, and artifact removal, the 8-m gridded DEM is optimal for further modeling and mapping. This DEM (Figure 1) includes about 33.5 million points (an elevation matrix of 7,199 × 4,675). Since REMA lacks bathymetry of the marine inlets, the number of points with elevation values is about 25.5 million.

Digital models of the nine most scientifically important morphometric variables were derived from the 8-m gridded DEM. The list of variables (Table 1) includes six local morphometric variables—slope gradient (G), slope aspect (A), horizontal curvature (k_h), vertical curvature (k_v), minimal curvature (k_{min}), and maximal curvature (k_{max}); one nonlocal variable—catchment area (S_{CA}); as well as two combined variables—topographic wetness index (I_{TWI}) and stream power index (I_{SPI}).

To derive digital models of local morphometric variables (G, A, k_h, k_v, k_{min}, and k_{max}), we applied the classical finite-difference Evans method (Evans, 1980). To compute a digital model of S_{CA}, we used the maximum-gradient based multiple flow direction algorithm (Qin et al., 2007) applied to a preprocessed sink-filled DEM. Since a very wide dynamic range of values characterizes S_{CA}, the digital model of S_{CA} was logarithmized. To derive digital models of combined morphometric variables (I_{TWI} and I_{SPI}), we used digital models of S_{CA} and G.

Details of definitions as well as physico-mathematical and physical-geographical interpretations of the mentioned morphometric variables can be found elsewhere (Florinsky, 2017, 2025a; Shary et al., 2002).

A hypsometric map of the Bunger Hills was created using the 8-m gridded DEM (Figure 1). Two gradient hypsometric tint scales were used to depict the topography:

1) To display the elevations of the oasis topography, we applied the green-yellow part of the standard spectral hypsometric scale of color plasticity (Kovaleva, 2014).

2) To display the elevations of the glacier topography, we utilized a modified hypsometric tint scale for polar regions (Patterson and Jenny, 2011).

Finally, hypsometric tinting was combined with achromatic hill shading derived from the DEM by a standard procedure (Figure 1).

From the calculated digital morphometric models, we produced a series of morphometric maps of the Bunger Hills at scales of 1∶150,000 and 1∶75,000 (Figures 1–7). For optimal perception of morphometric information, we used the following gradient tint scales:

- To map G (which can take only positive values from 0° to 90°), we applied a monochrome orange tint scale (the minimum and maximum G values correspond to least and most saturated orange shades, respectively) (Figure 2).
- To map k_h, k_v, k_{min}, and k_{max} (which can take both negative and positive values, having opposite physico-mathematical sense and interpretation), we used a two-color tint scale consisting of two contrasting parts, blue and orange (negative and positive values, respectively). The most and least saturated shades of blue or orange colors correspond to the absolute maximum and absolute minimum values, respectively, of k_h, k_v, k_{min}, and k_{max} (Figures 4–6).
- To map S_{CA} (which can take only positive values), we applied a standard gray tint scale (the minimum and maximum logarithmized S_{CA} values correspond to white and black, respectively) (Figure 7a).
- To map I_{TWI} and I_{SPI} (which can take only positive values), we applied a standard tint scale of spectral colors (the minimum and maximum values of I_{TWI} or I_{SPI} correspond to violet and red, respectively) (Figures 3 and 7b).
- To map A (which is circular variable taking values from 0° to 360°), we applied a color, eight-cardinal direction tint scale (Figure 8).

There is no lake bathymetry data in REMA, but unlike marine water bodies, lake cells are not marked as “no data”. These cells contain interpolated values of lake coastal elevations, that is, artifacts. In this regard, the lakes were masked on the resulting maps.

In addition, REMA contains multiple island-like artifacts, which are images of icebergs. On the produced maps, these artifacts located in marine inlets were also masked. To create masks, we used available topographic maps (Anonymous, 2005; Australian Antarctic Division, 2023; Knorozova and Korneeva, 1966) as reference data.

To compare the spatial distribution of G, k_h, k_v, k_{min}, k_{max}, S_{CA}, I_{TWI}, and I_{SPI} values within ice-free areas of the eastern and western parts of the southern Bunger Hills as well as northern peninsulas and islands, we carried out a descriptive linear statistical analysis of the derived morphometric models (Figure 9 and Table 2). To handle wide ranges of values of all curvatures and S_{CA}, their histograms were logarithmically transformed. All histograms were normalized to facilitate comparison of areas with different numbers of cells with calculated values of morphometric variables. To perform a comparison of spatial distribution of A values within those three areas, we constructed circular diagrams (Figure 10).

For DEM processing and geomorphometric calculations, we used a software SAGA 9.3.0 (Conrad et al., 2015). For mapping and statistical analysis, we utilized ArcGIS Pro 3.0.1.

4 Results and discussion

4.1 General results

Geomorphometric modeling and mapping resulted in a series of medium- to large-scale morphometric maps of the Bunger Hills (37 maps in total, each on A3 sheets):

1) A hypsometric map for the entire territory of the oasis and adjacent glaciers, scale 1∶150,000 (Figure 1).

2) Maps of G, A, k_h, k_v, k_{min}, k_{max}, S_{CA}, I_{TWI}, and I_{SPI} for:

• The entire territory of the Bunger Hills and adjacent glaciers, scale 1∶150,000.

• The southern Bunger Hills (western part), scale 1∶75,000 (Figures 2a and 3a).

• The southern Bunger Hills (eastern part), scale 1∶75,000 (Figures 2b and 3b).

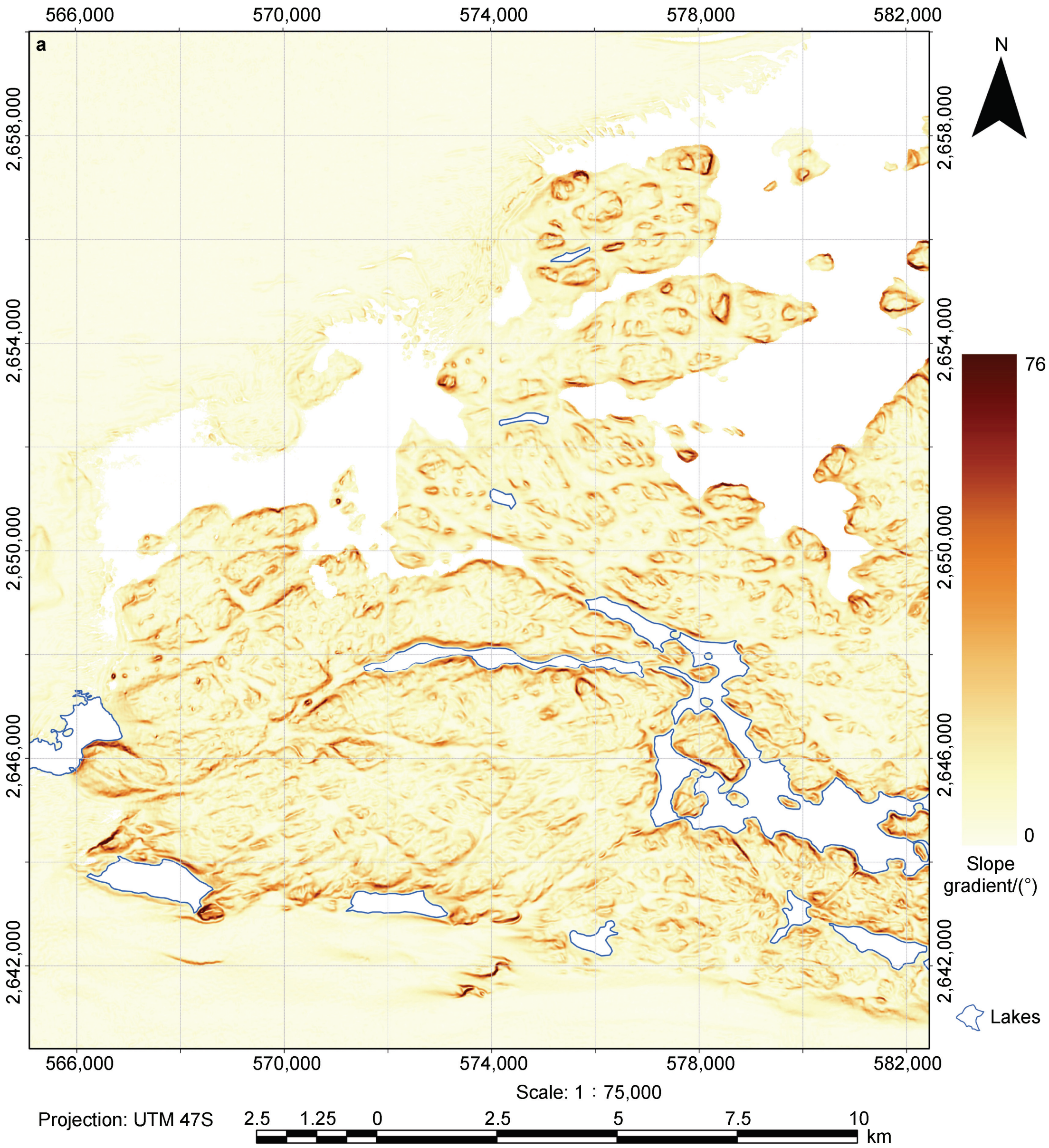

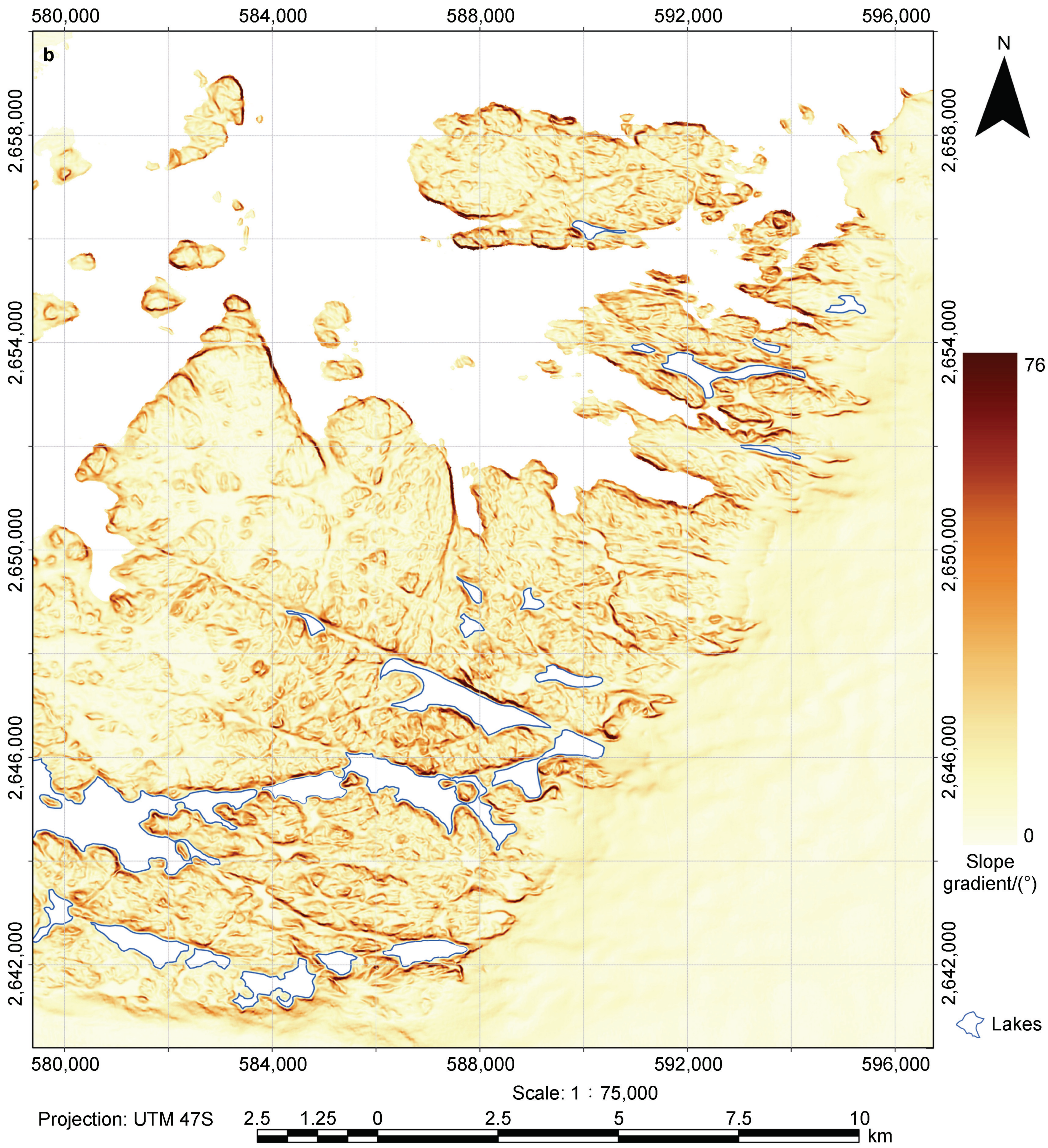

Figure 2 The slope gradient of the southern Bunger Hills (the 1 ∶ 75,000 scale maps). **a**, western part; **b**, eastern part.

• Booth (Charnockite) and Geomorfologov Peninsulas as well as Thomas Island, scale 1 ∶ 75,000 (Figures 4–8).

The use of two scales, as well as mapping the territory at a scale of 1 ∶ 75,000 on three charts, allowed the morphometric features of the Bunger Hills to be displayed in all their diversity and with varying levels of detail. Each morphometric map quantitatively describes a specific property of topography and has a unique physico-mathematical and physical-geographical interpretation (Florinsky, 2017, 2025a). The morphometric maps are conjugate and mutually complementary.

4.2 Local morphometry

All morphometric maps—in particular, the *G* maps (Figure 2)—demonstrate the spatial diversity and heterogeneity of the oasis topography. The most complex terrain can be found in the eastern part of the southern Bunger Hills including the Fuller (Kashalot) Island (Figures 2b and 3b) as well as on the Booth (Charnockite) Peninsula (Figures 4–7). Asymmetrical hills are widespread there, separated by numerous narrow valleys, the deepest parts of which are occupied by freshwater lakes. The western slopes of the hills are longer and gentler than the eastern slopes. This feature is most typical of the central part of the oasis, where the hills form a cuesta-like topography due to monoclinal occurrences of plagiogneisses and crystalline schists falling to the west and having a near-north strike (Bolshiyanov, 1990).

In the western part of the southern Bunger Hills (Figures 2a and 3a), the rock bedding elements are more varied, with steep or vertical bedding. The area is dominated by flat-topped hills with steep slopes that divide wide valleys.

The northern part of the Currituck (Geografov) Island and most of the Thomas Island (Figures 4 and 5) are characterized by a gentle topography. Local hills and ridges are leveled by loose debris material, which is represented by glacial, eluvial, and deluvial deposits (Bolshiyanov, 1990).

Results of the statistical analysis (Figure 9e and Table 2) showed that *G* generally follows a lognormal distribution, which differs insignificantly for the western/eastern parts of the southern Bunger Hills and northern peninsulas. The steepest surfaces can be found on the coast (rocky outcrops and cliffs dropping into the sea) as well as in areas of faults and intrusions (Tucker et al., 2020), while the gentlest surfaces are typical for the glaciers, especially the Edisto Glacier Tongue.

The *A* maps (Figure 8) describe the territory according to the slope orientations in eight cardinal directions. Statistically, in terms of *A* values' spatial distribution, the three subareas—the western and eastern parts of the southern Bunger Hills as well as the northern peninsulas/islands—are virtually indistinguishable (Figure 10). Slopes with northern and southern exposures predominate; slopes with western and eastern exposures are the least common; the prevalence of slopes with other exposures is intermediate. This is consistent with the fact that most of the hill chains and valleys between them are oriented along near-E-W, SE-NW, and NE-SW directions that in turn reflects the orientation of the local fault network (Ravich, 1960).

The k_h maps (Figure 4) display the distribution of convergence and divergence areas of surface flows ($k_h < 0$ and $k_h > 0$, respectively) (Florinsky, 2017, 2025a; Shary et al., 2002). Geomorphologically, these are spurs of valleys and crests, respectively (Figure 4, blue and orange shades, respectively). The combination of convergence and divergence

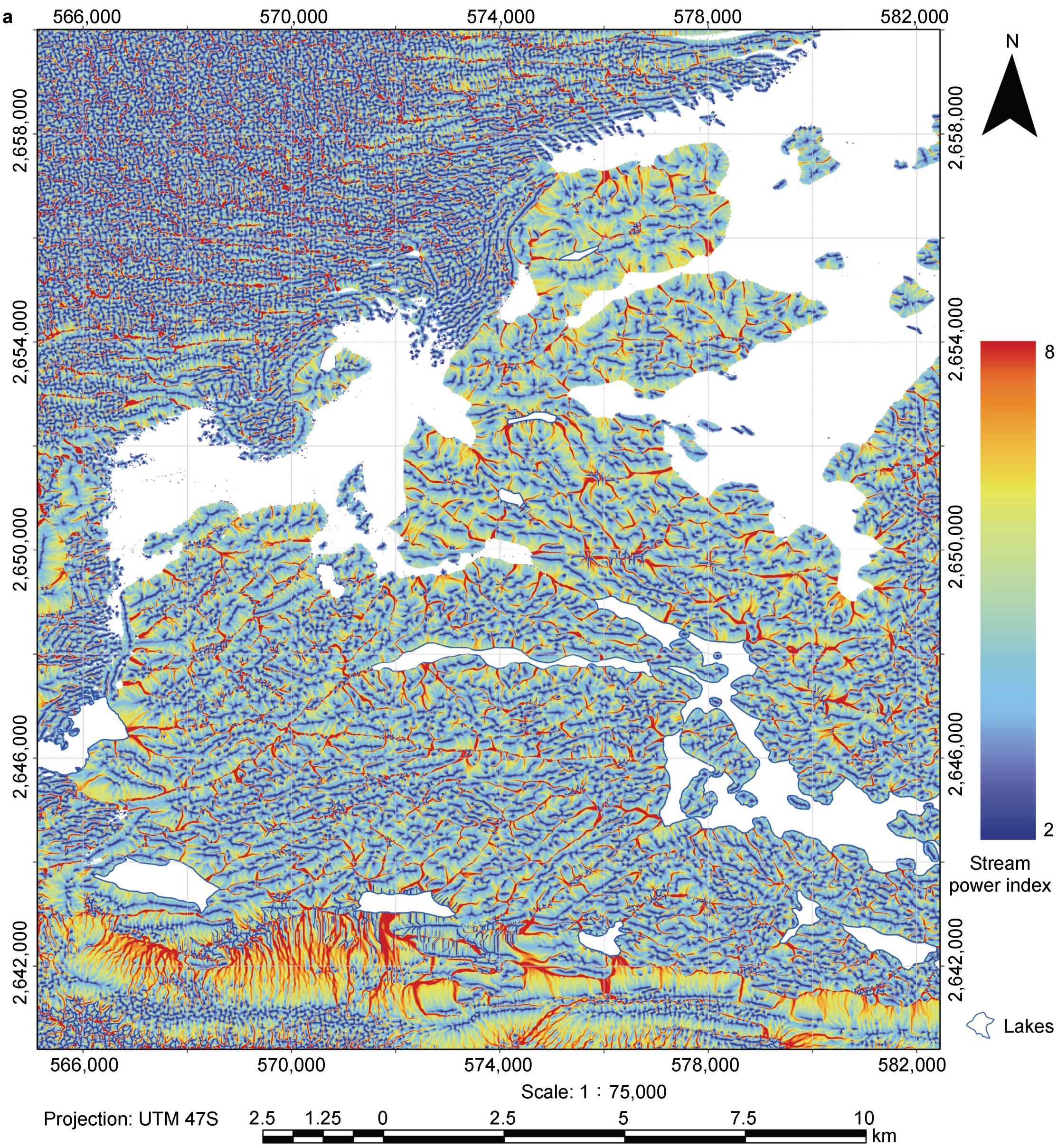

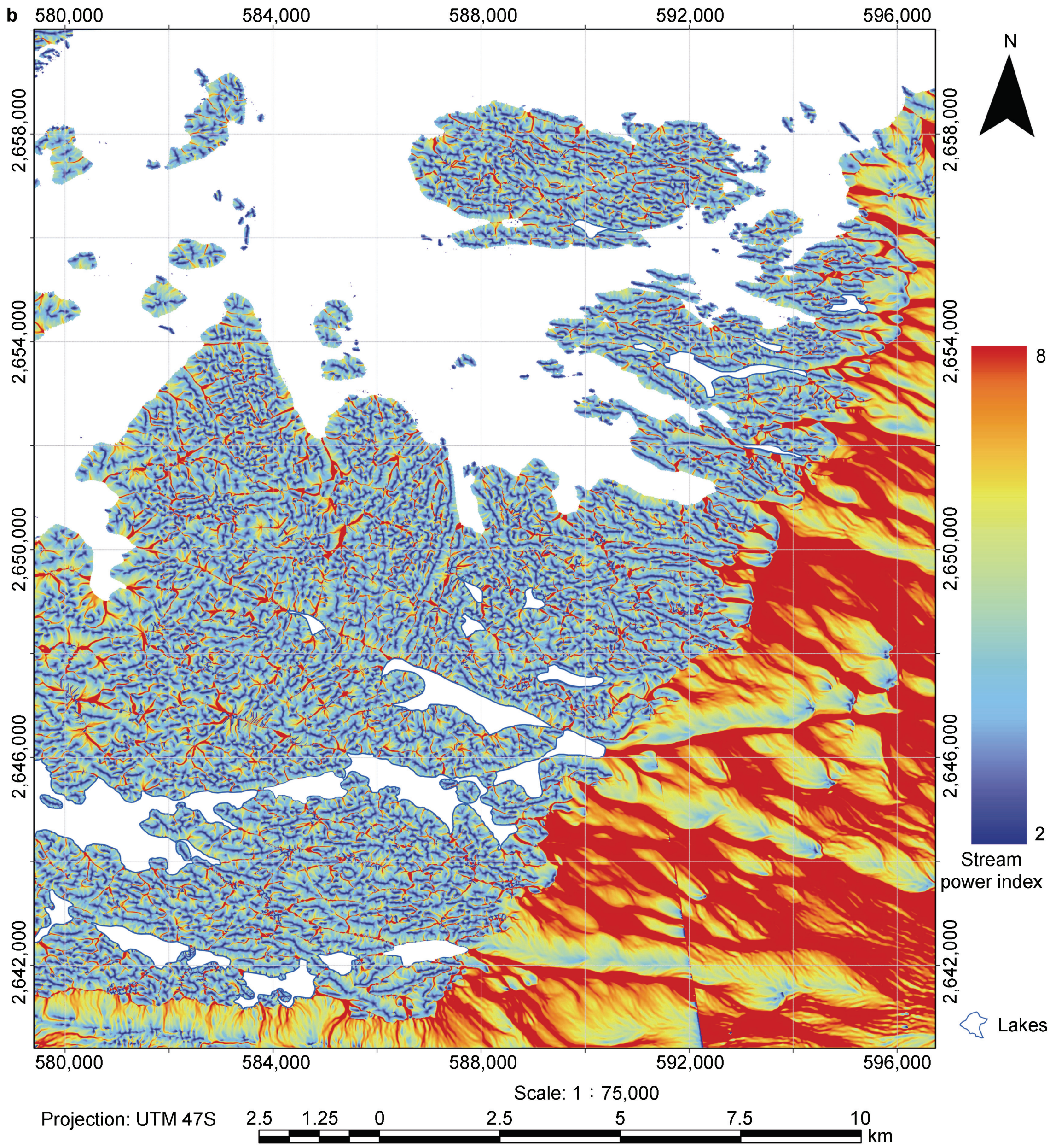

Figure 3 The stream power index of the southern Bunger Hills (the 1：75,000 scale maps). **a**, western part; **b**, eastern part.

areas creates an image of the flow structures, the configuration of which in the Bunger Hills is controlled by faults and fractures (Ravich, 1960).

In general, the structure and composition of the oasis topography are determined by the dense interweaving and intersection of valleys of different sizes. The confinement of the valleys to the faults (Ravich, 1960) indicates the leading role of endogenous processes in the formation and transformation of the Bunger Hills' valleys. The main, most probable exogenous factor of valley formation is erosion occurred before glaciation and during deglaciation of the oasis (Bolshiyanov, 1990). In fact, the fault network predetermined the subsequent directions of glacier movement, the drainage network patterns, and the location of lake basins.

The k_v maps (Figure 6a) show the distribution of relative deceleration and acceleration areas of flows ($k_v < 0$ and $k_v > 0$, blue and orange shades, respectively) (Florinsky, 2017, 2025a; Shary et al., 2002). Geomorphologically, this map represents cliffs, scarps, terrace edges, and other similar landforms or their elements with sharp bends in the slope profile.

The k_{max} and k_{min} maps (Figures 5 and 6b) are mainly informative in structural geological terms, because they reveal elongated linear landforms (Florinsky, 2017, 2025a). Concave elongated linear landforms (e.g., valleys) can be seen on k_{min} maps; they are displayed as dark blue lineaments (Figure 6b, $k_{min} < 0$). Convex elongated linear

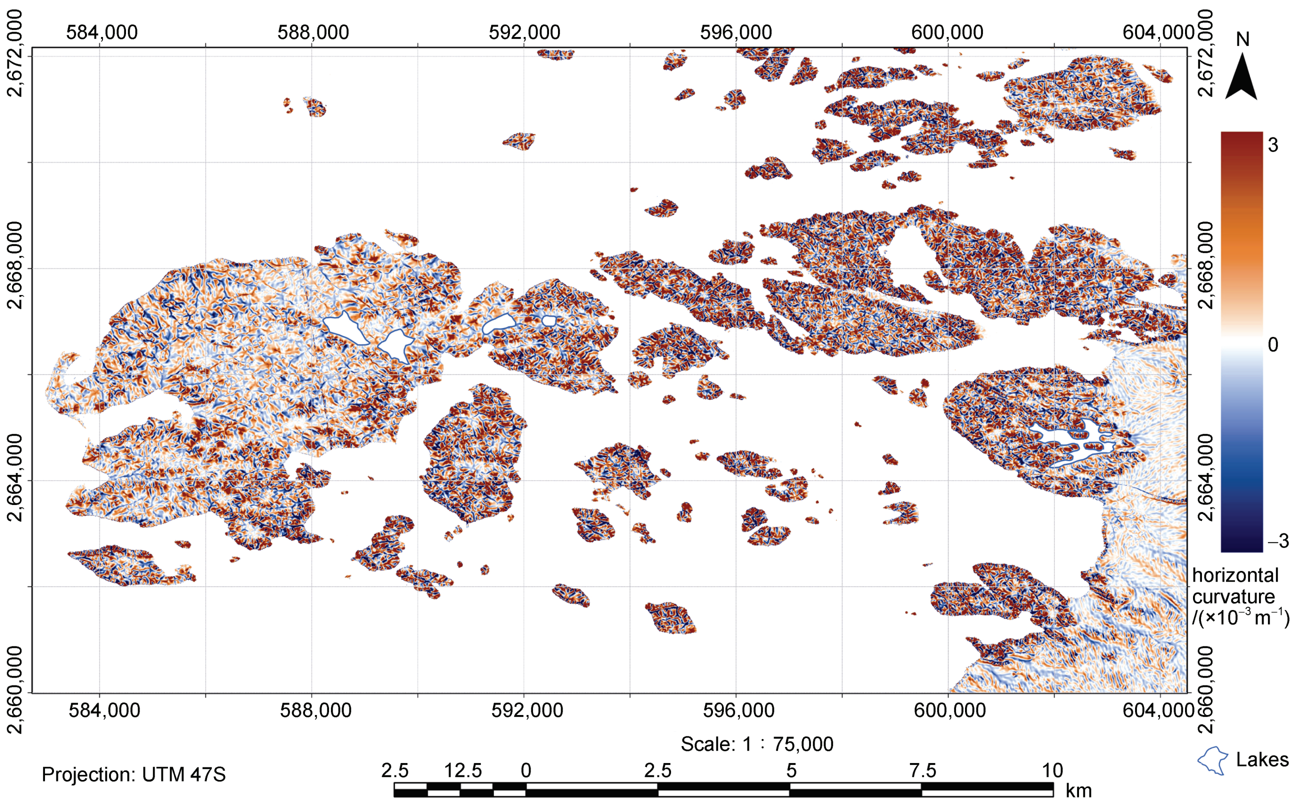

Figure 4 Booth (Charnockite) and Geomorfologov peninsulas as well as Thomas Island: horizontal curvature (the 1 : 75,000 scale map).

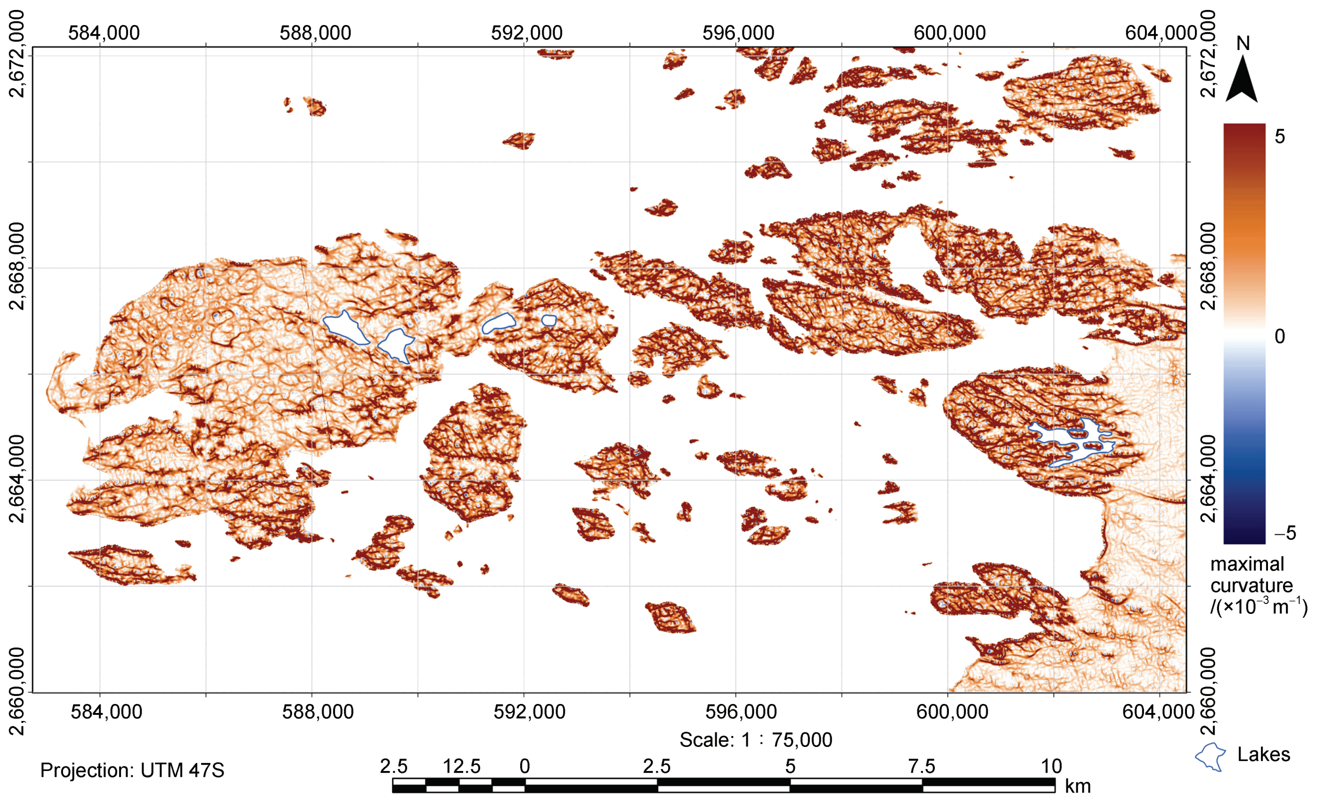

Figure 5 Booth (Charnockite) and Geomorfologov peninsulas as well as Thomas Island: maximal curvature (the 1 : 75,000 scale map).

Table 1 Formulas, definitions, and interpretations of selected morphometric variables (Florinsky, 2017, 2025a)

Variable, notation, and unit	Formula, definition, and interpretation
Slope gradient, G/(°)	$G = \arctan\sqrt{p^2+q^2}$ An angle between the tangential and horizontal planes at a given point of the topographic surface. Relates to the velocity of gravity-driven flows.
Slope aspect, A/(°)	$A = -90\left[1-\operatorname{sign}(q)\right]\left(1-\left\|\operatorname{sign}(p)\right\|\right)+180\left[1+\operatorname{sign}(p)\right]-\frac{180}{\pi}\operatorname{sign}(p)\arccos\left(\frac{-q}{\sqrt{p^2+q^2}}\right)$ An angle between the north direction and the horizontal projection of the two-dimensional vector of gradient counted clockwise, from 0° to 360°, at a given point of the topographic surface. Relates to the direction of gravity-driven flows.
Horizontal curvature, k_h/m^{-1}	$k_h = -\frac{q^2r-2pqs+p^2t}{\left(p^2+q^2\right)\sqrt{1+p^2+q^2}}$ A curvature of a normal section tangential to a contour line at a given point of the surface. A measure of flow convergence and divergence. Gravity-driven lateral flows converge where $k_h < 0$, and diverge where $k_h > 0$. k_h mapping reveals crest and valley spurs.
Vertical curvature, k_v/m^{-1}	$k_v = -\frac{p^2r+2pqs+q^2t}{\left(p^2+q^2\right)\sqrt{\left(1+p^2+q^2\right)^3}}$ A curvature of a normal section having a common tangent line with a slope line at a given point of the surface. A measure of relative deceleration and acceleration of gravity-driven flows. They are decelerated where $k_v < 0$, and are accelerated where $k_v > 0$. k_v mapping reveals terraces and scarps.
Minimal curvature, k_{min}/m^{-1}	$k_{min} = -\frac{\left(1+q^2\right)r-2pqs+\left(1+p^2\right)t}{2\sqrt{\left(1+p^2+q^2\right)^3}}-\sqrt{\frac{\left[\left(1+q^2\right)r-2pqs+\left(1+p^2\right)t\right]^2}{4\left(1+p^2+q^2\right)^3}-\frac{rt-s^2}{\left(1+p^2+q^2\right)^2}}$ A curvature of a principal section with the lowest value of curvature at a given point of the surface. $k_{min} > 0$ corresponds to local convex landforms, while $k_{min} < 0$ relates to elongated concave landforms (e.g., hills and troughs, correspondingly).
Maximal curvature, k_{max}/m^{-1}	$k_{max} = -\frac{\left(1+q^2\right)r-2pqs+\left(1+p^2\right)t}{2\sqrt{\left(1+p^2+q^2\right)^3}}+\sqrt{\frac{\left[\left(1+q^2\right)r-2pqs+\left(1+p^2\right)t\right]^2}{4\left(1+p^2+q^2\right)^3}-\frac{rt-s^2}{\left(1+p^2+q^2\right)^2}}$ A curvature of a principal section with the highest value of curvature at a given point of the surface. $k_{max} > 0$ corresponds to elongated convex landforms, while $k_{max} < 0$ relate to local concave landforms (e.g., crests and holes, correspondingly).
Catchment area, S_{CA}/m^2	An area of a closed figure formed by a contour segment at a given point of the surface and two flow lines coming from upslope to the contour segment ends. A measure of the contributing area.
Topographic wetness index, I_{TWI}	$I_{TWI} = \ln\left[1+\frac{S_{CA}}{10^{-3}+\tan G}\right]$ A ratio of catchment area to slope gradient at a given point of the topographic surface. A measure of the extent of flow accumulation.
Stream power index, I_{SPI}	$I_{SPI} = \ln\left(1+S_{CA}\cdot\tan G\right)$ A product of catchment area and slope gradient at a given point of the topographic surface. A measure of potential flow erosion and related landscape processes.

Note: $p=\frac{\partial z}{\partial x}$, $q=\frac{\partial z}{\partial y}$, $r=\frac{\partial^2 z}{\partial x^2}$, $t=\frac{\partial^2 z}{\partial y^2}$, $s=\frac{\partial^2 z}{\partial x \partial y}$ for $z=f(x,y)$, where z is elevation, and x and y are Cartesian coordinates.

landforms (e.g., crests) can be seen on k_{max} maps; they are displayed as dark orange lineaments (Figure 5, $k_{max} > 0$). These lineaments can be interpreted as a reflection of the local fault and fracture network, whose topographic manifestation has been amplified by erosional, exaration, and nival processes (Ravich, 1960).

Let us emphasize once again that in the Bunger Hills, the faults played a decisive role in the topography formation. Almost all the valleys and the shores of the sea bays are laid along the lines of faults (Ravich, 1960). This can indicate that the oasis territory is divided by faults into numerous blocks that may experience differentiated vertical tectonic movements (Bolshiyanov, 1990).

The statistical analysis of the curvature models (Figures 9a–9d and Table 2) expectedly showed that they generally follow distorted normal distributions. For k_h and k_v, distribution curves are located more or less symmetrically relative to the zero value (Figures 9a, 9b). For k_{min} and k_{max}, distribution curves are skewed to the negative and positive sides, respectively (Figures 9c, 9d). Such a statistical behavior is typical for these morphometric variables (Florinsky, 2025a). Curvature distribution curves (Figures 9a–9d) demonstrate certain differences for the western/eastern parts of the southern Bunger Hills and northern peninsulas (especially k_h and k_v). These differences relate mainly to values, which are relatively close to zero; that is, these three subareas differ in the morphometry of relatively flat sites. A more detailed interpretation of this result can require an additional study.

4.3 Nonlocal and combined morphometry

S_{CA} is a measure of the area of land surface that can be drained through a given point of the surface (Florinsky, 2017, 2025a). On the S_{CA} maps (Figure 7a), the crests and

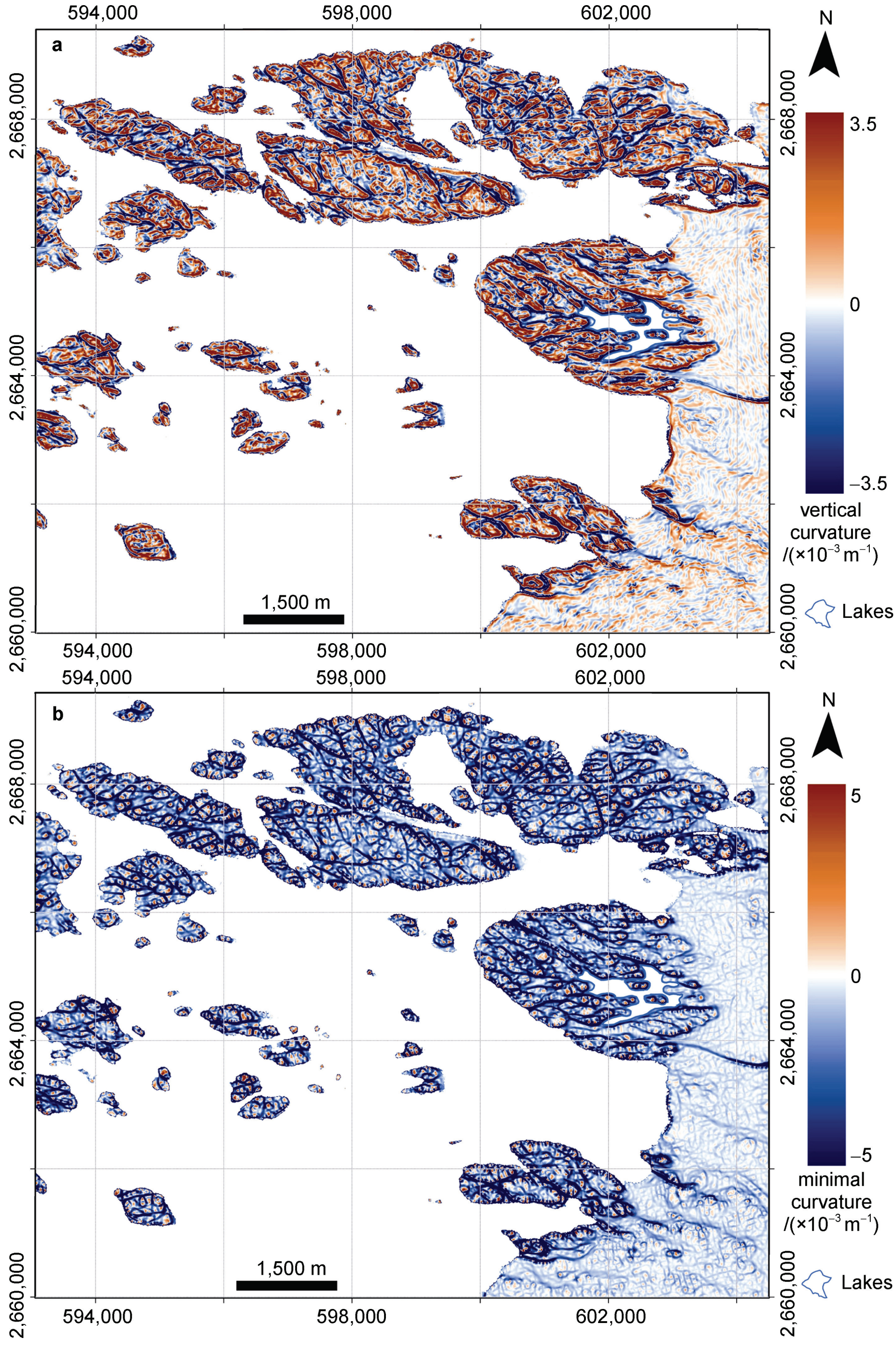

Figure 6 The vertical curvature (**a**) and minimal curvature (**b**) of Booth (Charnockite) and Geomorfologov Peninsulas (parts of the 1 ∶ 75,000 scale maps; projection UTM 47S).

thalwegs are clearly visible as light and dark lines, respectively (low and high S_{CA} values, respectively). S_{CA} maps can be used to identify drainage basins and then to incorporate this information into geochemical or hydrological analysis.

I_{TWI} and I_{SPI} are functions of S_{CA} and G (Table 1). I_{TWI} is a measure of the degree of surface flow accumulation (Florinsky, 2017, 2025a). The higher the S_{CA} value and the lower the G value, the higher the I_{TWI} value and the greater the potential moisture accumulation in the near-surface layer. In the study area, maximum values of I_{TWI} correspond to glacial streams on the ice sheet and the Edisto Glacier

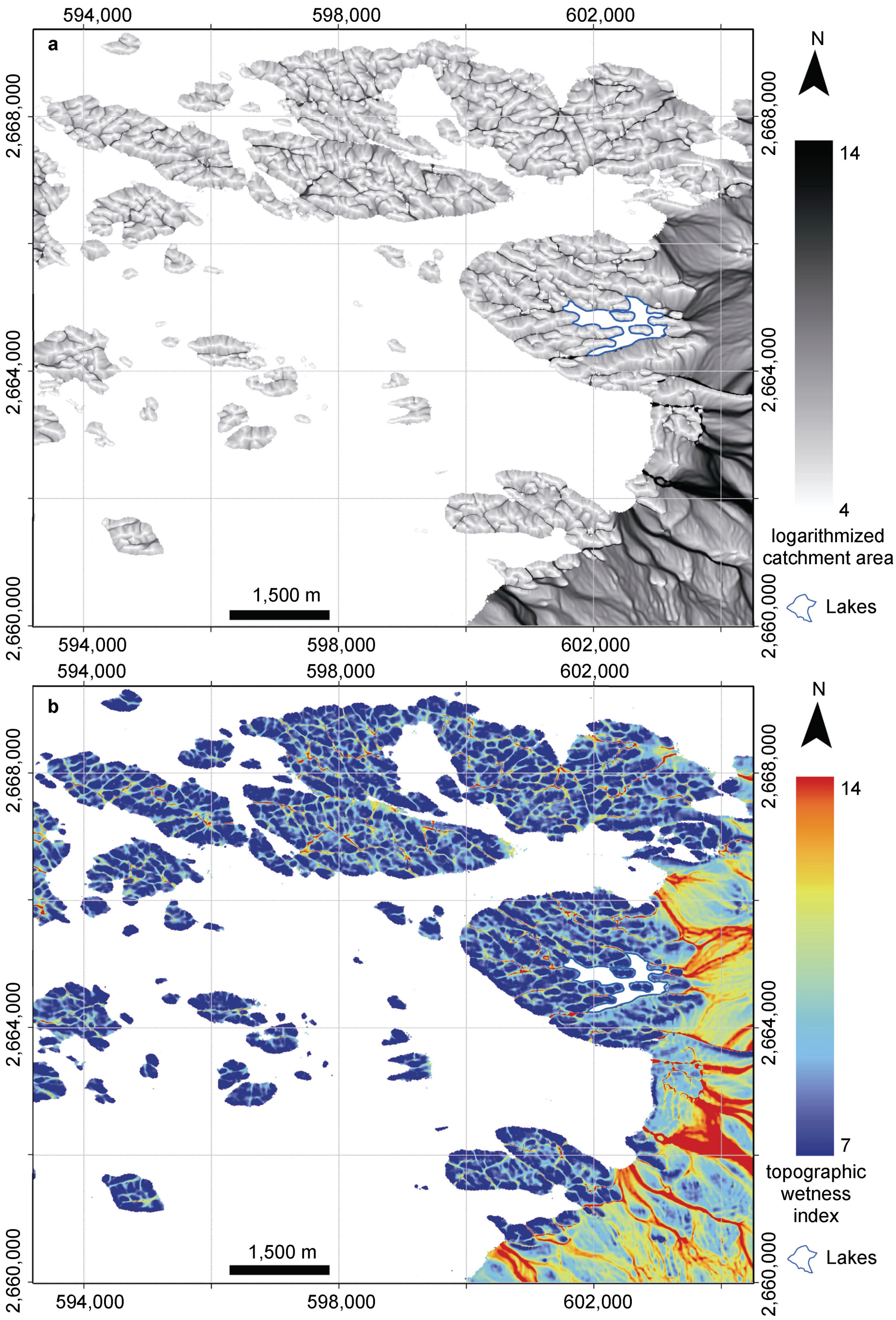

Figure 7 The logarithmized catchment area (**a**) and topographic wetness index (**b**) of Booth (Charnockite) and Geomorfologov peninsulas (parts of the 1∶75,000 scale maps; projection UTM 47S).

Tongue, as well as seasonal stream valleys of the oasis. The I_{TWI} maps (Figure 7b) can be used for spatial prediction of the ground moisture content in the oasis as well as for forecasting the spatial distribution of snow puddles on glaciers in austral summer.

I_{SPI} is a measure of the potential erosive force of surface flows (Florinsky, 2017, 2025a). The higher the S_{CA} value and the G value, the higher the I_{SPI} value. In the study area, its minimum values correspond to the flow structures of the Edisto outlet glacier and the Shackleton Ice Shelf, while its maximum values relate to the flow structures of the ice sheet. The I_{SPI} maps (Figure 3) can be useful for

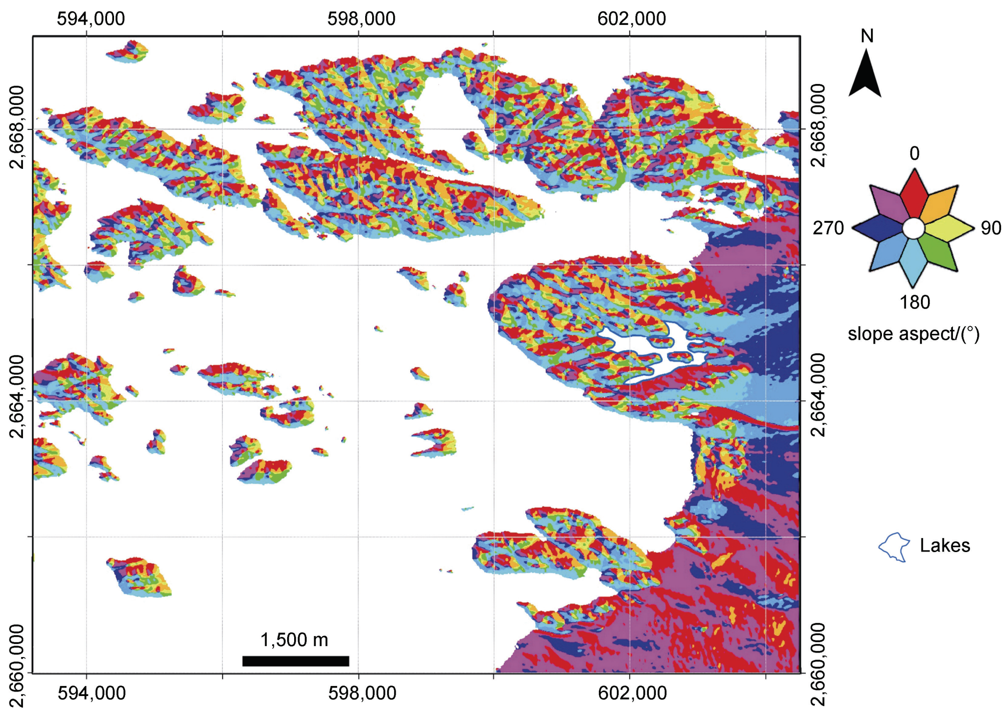

Figure 8 Booth (Charnockite) and Geomorfologov peninsulas: slope aspect (parts of the 1∶75,000 scale maps; projection UTM 47S).

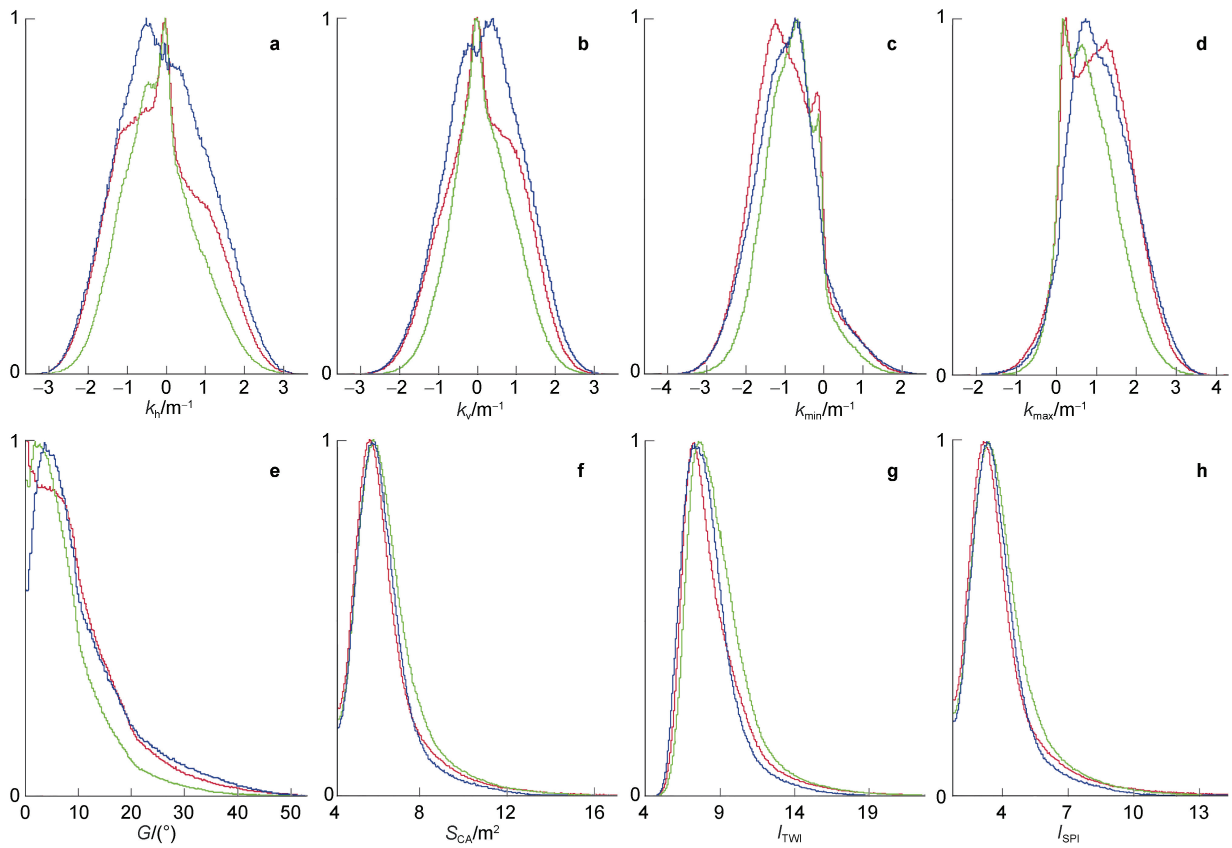

Figure 9 Distribution of morphometric variable values for the western part of the southern Bunger Hills (red), eastern part of the southern Bunger Hills (green), as well as northern peninsulas and islands (blue). **a**, horizontal curvature; **b**, vertical curvature; **c**, minimal curvature; **d**, maximal curvature; **e**, slope gradient; **f**, catchment area; **g**, topographic wetness index; **h**, stream power index. *X*-axes, values of morphometric variables; *Y*-axes, normalized numbers of cells.

Table 2 Descriptive statistics of morphometric variables for ice-free areas of the western part of the southern Bunger Hills (SW), eastern part of the southern Bunger Hills (SE), as well as northern peninsulas and islands (N)

Morphometric variable	Area	Statistics			
		Minimum	Maximum	Average	Standard deviation
Horizontal curvature, k_h/m^{-1}	SW	−0.042	0.05	0	0.0025
	SE	−0.077	0.068	0	0.0018
	N	−0.063	0.058	0	0.0025
Vertical curvature, k_v/m^{-1}	SW	−0.035	0.038	0	0.0024
	SE	−0.051	0.059	0	0.0033
	N	−0.041	0.043	0	0.0033
Minimal curvature, k_{min}/m^{-1}	SW	−0.105	0.027	−0.001	0.0024
	SE	−0.109	0.029	−0.001	0.0035
	N	−0.093	0.018	−0.001	0.0035
Maximal curvature, k_{max}/m^{-1}	SW	−0.022	0.177	0.001	0.0026
	SE	−0.04	0.132	0.001	0.0036
	N	−0.021	0.119	0.001	0.0038
Slope gradient, G/(°)	SW	0	76.8	7.8	7
	SE	0	70.1	9.8	8.7
	N	0	75.5	11	9.1
Catchment area, S_{CA}/m^2	SW	4.17	19.21	6.62	1.72
	SE	4.17	19.05	6.49	1.82
	N	4.17	16.83	6.33	1.38
Topographic wetness index, I_{TWI}	SW	2.77	26.08	9.08	2.27
	SE	3.57	25.77	8.73	2.4
	N	2.87	22.33	8.32	1.85
Stream power index, I_{SPI}	SW	1.74	18.15	4.47	1.56
	SE	1.74	17.99	4.31	2.04
	N	1.74	15.63	4.14	2.41

spatial prediction of slope erosion in the oasis as well as erosion of snow cover and ice by meltwater flows on glaciers in austral summer.

Mapping of S_{CA}, I_{TWI}, and I_{SPI} (Figures 3b and 7) allowed revealing a system of ice flows of the Antarctic Ice Sheet margin. They are most clearly visualized as red tail-like patterns on the I_{SPI} maps (Figure 3b). S_{CA}, I_{TWI}, and I_{SPI} maps make it possible to analyze the spatial configuration of these ice flows.

For outlet glaciers, S_{CA}, I_{TWI}, and I_{SPI} maps reveal predominantly a complex network of crevasses, which is especially noticeable on the Edisto Glacier Tongue (Figure 3a). Crevasses appear as relatively parallel, thin curved red lines on a blue-light blue background.

The statistical analysis (Figures 9f–9h and Table 2) expectedly showed that S_{CA}, I_{TWI}, and I_{SPI} models follow lognormal distributions, which are almost identical for the western and eastern parts of the southern Bunger Hills as well as northern peninsulas.

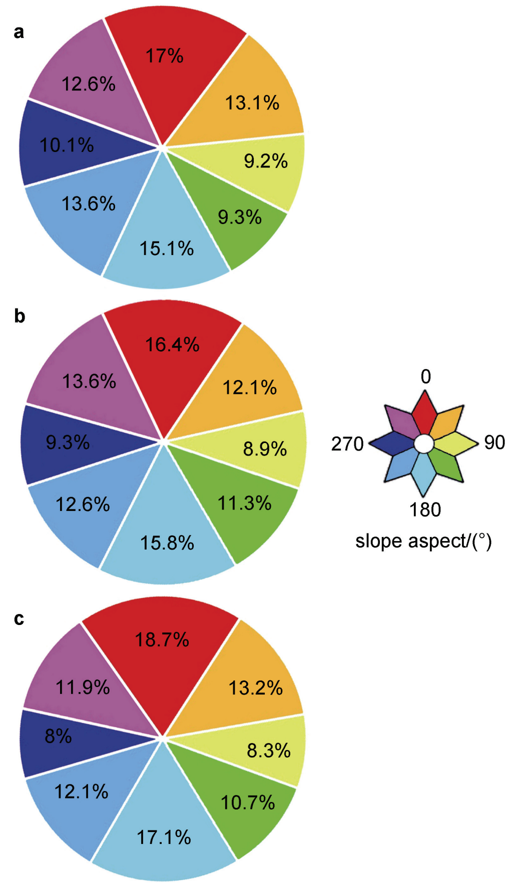

Figure 10 Distribution of slope aspect values for (**a**) the western part of the southern Bunger Hills, (**b**) eastern part of the southern Bunger Hills, and (**c**) northern peninsulas and islands.

4.4 Morphometry, snow accumulation, and permafrost

Let us describe a particular impact of quantitative characteristics of topography (morphometric variables) on snow accumulation and permafrost dynamics.

In the Bunger Hills, the snow accumulation period lasts from February to November. In calm weather, the snow cover evenly covers the entire oasis. However, during strong wind gusts, snow is blown off the steep, screwed slopes and deposited mainly on the western and northwestern leeward slopes, forming massive perennial snowfields. They reach 150–200 m in length, 60 m in width, and 10–15 m in thickness (Grigoriev, 1966). Such snowfields are typical for the central part of the southern Bunger Hills.

At the same time, seasonal snowdrifts are common on the windward slopes, differing in shape and size from the large snowfields on the leeward slopes. Snowdrifts are located both at the foot of the slopes and at different altitudes. They often lie on the slopes in several tiers outlining terraces. Strips of snowdrifts are usually several meters wide, several tens of meters long, and 1–5 m thick (Grigoriev, 1966). Snowdrifts form annually; most of them melt by the end of summer.

Perennial snowfields affect the underlying permafrost rocks by influencing temperature and thickness of the permafrost layer. In summer, the snow cover prevents heat from penetrating to the underlying rock surface, while in winter, the snow cover prevents radiating heat into the atmosphere from underlying rocks. The heat-insulating properties of perennial snowfields cause an increase in the temperature in the underlying rocks, compared to snowfield-free areas. In the Bunger Hills, the average annual air temperature is −8.4 ℃, while the average annual temperature of rocks at a depth of 1.2 m is −7.7 ℃ within the ice-free areas. The thickness of the permafrost layer in these areas is estimated to be about 130–150 m, while that under perennial snowfields is much greater (Grigoriev, 1966).

In the Bunger Hills, rocks under snowfields are frozen throughout the summer. Formation of a seasonally thawing layer under seasonal snowfields begins after the ground surface is cleared of snow. A snowfield usually affects the decrease in the depth of rock thawing in a strip 10–12 m wide from the snowfield edge. Within this strip, the depth of seasonal thawing fluctuates between 0.2 and 0.5 m. While outside the snowfield influence, the depth of seasonal rock thawing is usually 1.6–1.7 m (Grigoriev, 1966).

The melting of seasonal and perennial snowfields causes intensive nivation, which in some cases leads to the formation of rudimentary cirques. In addition, the water from melting snowfields accumulating on the surface of the permafrost layer contributes to solifluction processes on the hill slopes. The accumulation of this water at the depressions and its freezing in winter lead to the formation of patterned grounds and small frost heave mounds (Grigoriev, 1966).

Let us analyze quantitative characteristics of the topography influencing the processes described above. First, it is obvious that the formation of both perennial snowfields and seasonal snowdrifts depends on the prevailing wind direction(s) and is directly influenced by two morphometric variables, such as slope gradient and slope aspect (Florinsky, 2025a; Hengl and Reuter, 2009).

Second, it is well known that the thermal regime of slopes is also controlled by these morphometric variables (Florinsky, 2025a; Hengl and Reuter, 2009; Shary et al., 2002). Therefore, the probability and speed of melting of snowfields and thawing of permafrost also depend on slope gradient and slope aspect. In particular, the warmest slopes are northern, northwestern, and northeastern ones (in descending order of warming).

Third, the direction and character of migration and accumulation of melting water from snowfields are determined by horizontal and vertical curvatures, which control two mechanisms of migration and accumulation of surface and near-surface gravity-driven flows: horizontal curvature controls flow convergence and divergence, while vertical curvature controls relative deceleration and acceleration of flows (Florinsky, 2025a; Shary et al., 2002). In addition, topographic wetness index—a measure of the extent of flow accumulation—can describe migration paths of melting water (and thus areas where solifluction processes can develop) as well as zones of moisture accumulation where patterned grounds and frost heave mounds can form.

We believe that the use of morphometric models can optimize both fundamental studies of permafrost dynamics and practical tasks of predicting snow accumulation, which may be relevant for organizing the life of wintering polar stations.

4.5 Accuracy, errors, and artifacts

It is well known that any DEM contains inevitable high-frequency noise, errors, and artifacts of various origins (Florinsky, 2025a). In the case of REMA (Howat et al., 2019), there are several sources of noise, errors, and artifacts as follows:

1) Possible insufficient quality of original satellite images, which can particularly be associated with spacecraft and sensor stability as well as the influence of the atmosphere and weather conditions at the time of acquiring the imagery (e.g., snow cover and clouds).

2) Errors in photogrammetric processing of the original stereoscopic imagery.

3) Errors in merging of initial multi-temporal strip DEMs into mosaic DEMs including interpolation errors.

4) Errors in editing/filtering of mosaic DEMs (e.g., an edited DEM contains island-like artifacts corresponding to icebergs).

5) Interpolation errors arising in a DEM if a user changes the polar stereographic projection of a REMA fragment into another projection.

However, to date, REMA is the most accurate DEM of Antarctica with absolute errors less than 1 m over most of the coverage area, and relative errors of a decimeter range (Polar Geospatial Center, 2023). A user needs to be aware of possible errors and artifacts and their sources and be critical of the products derived from REMA because all DEM-derived morphometric models and maps always inherit and even amplify the severity of DEM errors.

Being functions of partial derivatives of elevation (Table 1), k_h, k_v, k_{min}, and k_{max} are sensitive to minor changes in elevation values including high-frequency noise and artifacts (Florinsky, 2025a). The use of noisy DEMs for modeling and calculations without preliminary filtering does not make sense, since the resulting morphometric maps will be unreadable (the noise will suppress the signal).

The selected fragment of the 8-m gridded REMA is marked by sufficient smoothness, a small number of artifacts, and the absence of pronounced high-frequency noise, as evidenced by the good readability of the generated morphometric maps. We did not perform an additional smoothing or filtering of the used DEM or produced digital morphometric models.

Notice that the sensitivity of morphometric values to minor changes in elevation values is also responsible for the following effect, which is not associated with calculation errors. Patterns of morphometric maps for the oasis and adjacent glaciers differ significantly from each other (Figures 2–7). This contrast, clearly visible to the naked eye, is associated, on the one hand, with the high level of smoothness of the glacier surface and, on the other hand, with the roughness and dissection of the ice-free surface of the oasis. In this regard, there is potential for future geomorphometric studies using multiscale calculation and mapping of surface roughness (Trevisani and Guth, 2024; Trevisani et al., 2023).

At the same time, all the produced maps contain a pronounced artifact in the form of a "lineament", which runs from south-southeast to north-northwest, crossing the Antarctic Ice Sheet margin in the southeast corner of the study area, then a portion of the southern Bunger Hills adjacent to the Kinzhal Bay, and finally the Fuller (Kashalot) and Thomas Islands (Figures 2b, 3b, 4 and 5). This "lineament" is a trace of stitching of two adjacent REMA tiles. This artifact can only be eliminated by manually editing the DEM.

Finally, let us note that a user should clearly understand the difference between the grid spacing and resolution of a DEM or a digital morphometric model (Florinsky, 2025a ; Guth et al., 2021): The grid spacing is a distance between two neighboring grid nodes of a regular model grid, which is measured along a grid row or column, while the resolution is the planimetric sizes of the smallest topographic feature detectable in a model. For the used fragment of REMA, for example, the DEM grid spacing is 8 m. However, according to the sampling theorem (Florinsky, 2025a), the DEM resolution of the REMA fragment is at least 16 m. This applies to all morphometric models derived from the DEM. This fact imposes obvious limitations on the real sizes of landforms displayed on morphometric maps and their interpretation. All map patterns smaller than 16 m are a reflection of high-frequency noise, which cannot be effectively removed or filtered. If a user plans to study microtopography with typical sizes of, say, 4 m, it is necessary to use morphometric maps derived from a DEM with a grid spacing $\leqslant$ 2 m.

5 Conclusions

We performed geomorphometric modeling of the Bunger Hills and created a set of medium- to large-scale morphometric maps of this ice-free Antarctic territory. The resulting morphometric maps quantitatively, rigorously, and reproducibly describe the topography of the oasis. This map series complements previously created topographic (Anonymous, 2005; Australian Antarctic Division, 2023; Battke, 1985; Knorozova and Korneeva, 1966), geological (Ravich and Solovyev, 1966; Sheraton and Tingey, 1994), permafrost-geomorphological (Grigoriev and Evteev, 1966), and glacial-geomorphological (Bolshiyanov, 1990) maps.

The geomorphometric modeling and mapping allowed the Bunger Hills topography to be displayed in all its diversity. Each morphometric map quantitatively describes a specific property of topography and has a unique physico-mathematical and physical-geographical interpretation. The derived morphometric maps are conjugate and mutually complementary.

We believe that new morphometric information may be useful both for refining existing geological, permafrost, and glacial geomorphological data for the Bunger Hills, and for further geological, geomorphological, permafrost, glaciological, hydrological, and ecological studies of this area.

However, prospective researchers should use morphometric digital data critically and remember that morphometric models and maps always contain certain errors, high-frequency noise, and artifacts that are inherited from the DEM and can be amplified by geomorphometric calculations. It is also necessary to keep in mind the resolution limitation of the morphometric materials, which is determined by the REMA grid spacing and the sampling theorem. The study was performed within the framework of the project to create a thematic physical-geographical scientific reference geomorphometric atlas of ice-free areas of Antarctica (Florinsky, 2024, 2025b).

Acknowledgments We gratefully acknowledge the valuable comments, suggestions, and recommendations of one anonymous reviewer, Dr. Kátia Kellem da Rosa as reviewer and Associate Editor Dr. Duncan Young.

References

Alexandrov M V. 1985. Landscape structure and mapping of the Enderby Land oases. Leningrad: Hydrometeoizdat (in Russian).

Anonymous. 2005. Bunger Oasis, 1:100,000 scale map//Korotkevich E S, Fomchenko V D, Fridman B S (eds). Atlas of the oceans: Antarctica. St. Petersburg: Main Department of Navigation and Oceanography, 62-63 (in Russian).

Australian Antarctic Division. 2023. Denman Terrestrial Campaign. Map 2: Bunger Hills, 1:200,000 scale map. Kingston: Australian Antarctic Division.

Avsyuk G A, Markov K K, Shumskiy P A. 1956. Geographical observations in the Antarctic 'oasis'. Proc Soviet Geograp Soc, 88(4): 316-350 (in Russian).

Bardin V I. 1970. Oases of Antarctica. Moscow: Znanie (in Russian).

Battke Z. 1985. Elaboration of topographic maps of the Polish A.B. Dobrowolski Station at Bunger Oasis on the Antarctic continent. Pol Polar Res, 6(3): 385-390.

Bockheim J G (ed). 2015. The soils of Antarctica. Cham: Springer, doi: 10.1007/978-3-319-05497-1.

Bolshiyanov D Y. 1990. Main features of the geomorphological structure of the Bunger Oasis (East Antarctica). Information Bulletin of the Soviet Antarctic Expedition, 113: 79-90 (in Russian).

Bölter M, Beyer L, Stonehouse B. 2002. Antarctic coastal landscapes: characteristics, ecology and research//Beyer L, Bölter M (eds). Geoecology of Antarctic ice-free coastal landscapes. Berlin, Heidelberg:

Springer Berlin Heidelberg, 5-15, doi: 10.1007/978-3-642-56318-8.
Byrd R E. 1947. Our Navy explores Antarctica. Nat Geo, 92(4): 429-522.
Conrad O, Bechtel B, Bock M, et al. 2015. System for Automated Geoscientific Analyses (SAGA) v.2.1.4. Geosci Model Dev, 8(7): 1991-2007, doi: 10.5194/gmd-8-1991-2015.
Evans I S. 1980. An integrated system of terrain analysis and slope mapping. Z Fur Geomorphol Suppl, 36: 274-295.
Florinsky I V. 2017. An illustrated introduction to general geomorphometry. Prog Phys Geogr Earth Environ, 41(6): 723-752, doi: 10.1177/0309133317733667.
Florinsky I V. 2023a. Geomorphometric modeling and mapping of Antarctic oases. ArXiv Preprints, 2305.07523: 1-84, doi: 10.48550/arXiv.2305.07523.
Florinsky I V. 2023b. Larsemann Hills: geomorphometric modeling and mapping. Polar Sci, 38: 100969, doi: 10.1016/j.polar.2023.100969.
Florinsky I V. 2024. A project of a geomorphometric atlas of ice-free Antarctic territories. InterCarto InterGIS, 30(2): 53-79, doi: 10.35595/2414-9179-2024-2-30-53-79 (in Russian with English abstract).
Florinsky I V. 2025a. Digital terrain analysis, 3rd rev. enl. edn. London: Academic Press, doi: 10.1016/C2023-0-51092-4.
Florinsky I V. 2025b. Geomorphometric atlas of Antarctic periglacial territories: structure, content, examples. Perugia, Italy: Proceedings of Geomorphometry 2025, 9–13 June 2025, doi: 10.5281/zenodo.14954567.
Gibson J A E. 2006. The environment of the Bunger Hills – 1999–2000, Ver. 1. Australian Antarctic Data Centre. (2022-08-18) [2025-05-06]. https://data.aad.gov.au/dataset/883CEFAA-CACB-4E61-8EA2-8937BB1B5F57.
Gibson J A E, Gore D B, Kaup E. 2002. Algae River: an extensive drainage system in the Bunger Hills, East Antarctica. Polar Rec, 38(205): 141-152, doi: 10.1017/s0032247400017526.
Gore D B, Rhodes E J, Augustinus P C, et al. 2001. Bunger Hills, East Antarctica: ice free at the Last Glacial Maximum. Geology, 29(12): 1103, doi: 10.1130/0091-7613(2001)029<1103:bheaif>2.0.co;2.
Grigoriev N F. 1962. Formation of topography and frozen rocks of the coast of East Antarctica. Moscow: Soviet Academic Press (in Russian).
Grigoriev N F. 1966. Snowfields of the Bunger Oasis and their role in the change of topography and the development of cryogenic phenomena in East Antarctica. Materials of Glaciological Studies, 12: 115-121 (in Russian).
Grigoriev N F, Evteev S A. 1966. Permafrost geomorphological map of the Bunger Oasis, 1:150,000 scale//Bakaev V G, Tolstikov E I (eds). Atlas of Antarctica, Vol. I. Moscow: Central Board of Geodesy and Cartography, 165-165 (in Russian).
Guth P L, Van Niekerk A, Grohmann C H, et al. 2021. Digital elevation models: terminology and definitions. Remote Sens, 13(18): 3581, doi: 10.3390/rs13183581.
Hengl T, Reuter H I (eds). 2009. Geomorphometry: concepts, software, applications. Amsterdam: Elsevier, doi: 10.1016/S0166-2481(08)00036-6.
Howat I M, Porter C, Smith B E, et al. 2019. The reference elevation model of Antarctica. Cryosphere, 13(2): 665-674, doi: 10.5194/tc-13-665-2019.
Howat I M, Porter C, Smith B E, et al. 2022. The Reference Elevation Model of Antarctica – Mosaics, Version 2. (2024-10-20) [2025-05-07]. https://doi.org/10.7910/DVN/EBW8UC.
Knorozova V N, Korneeva E Z. 1966. Bunger Oasis, 1:100,000 scale map//Bakaev V G, Tolstikov E I (eds). Atlas of Antarctica, Vol. I. Moscow: Central Board of Geodesy and Cartography, 163-164 (in Russian).
Korotkevich E S. 1972. Polar deserts. Leningrad: Hydrometeoizdat (in Russian).
Kovaleva O V. 2014. Perfecting the relief presentation by hypsometric painting. New classification of hypsometric scales. Geod Cartogr, 893(11): 21-29, doi: 10.22389/0016-7126-2014-893-11-21-29.
Lv G N, Xiong L Y, Chen M, et al. 2017. Chinese progress in geomorphometry. J Geogr Sci, 27(11): 1389-1412, doi: 10.1007/s11442-017-1442-0.
Markov K K, Bardin V I, Lebedev V L, et al. 1970. The geography of Antarctica. Jerusalem: Israel Program for Scientific Translations.
Minár J, Krcho J, Evans I S. 2016. Geomorphometry: quantitative land-surface analysis//Elias S A (ed). Reference module in earth systems and environmental sciences. Amsterdam: Elsevier, doi: 10.1016/B978-0-12-409548-9.10260-X.
Moore I D, Grayson R B, Ladson A R. 1991. Digital terrain modelling: a review of hydrological, geomorphological, and biological applications. Hydrol Process, 5(1): 3-30, doi: 10.1002/hyp.3360050103.
Ochyra R, Lewis Smith R I, Bednarek-Ochyra H. 2008. Illustrated moss flora of Antarctica. Cambridge: Cambridge University Press.
Øvstedal D O, Lewis Smith R I. 2001. Lichens of Antarctica and South Georgia: a guide to their identification and ecology. Cambridge: Cambridge University Press.
Patterson T, Jenny B. 2011. The development and rationale of cross-blended hypsometric tints. Cartogr Perspect, (69): 31-46, doi: 10.14714/cp69.20.
Pickard J (ed). 1986. Antarctic oasis, terrestrial environment and history of the Vestfold Hills. New York: Academic Press.
Polar Geospatial Center. 2023. Guide: PGC's DEM Products – ArcticDEM, REMA, and EarthDEM. Saint Paul: Polar Geospatial Center, University of Minnesota. (2025-03-21) [2025-05-07]. https://www.pgc.umn.edu/guides/stereo-derived-elevation-models/pgcs-dem-products-arcticdem-rema-and-earthdem.
Qin C, Zhu A X, Pei T, et al. 2007. An adaptive approach to selecting a flow-partition exponent for a multiple-flow-direction algorithm. Int J Geogr Inf Sci, 21(4): 443-458, doi: 10.1080/13658810601073240.
Ravich M G. 1957. Rocks of the Bunger Oasis. Proceedings of the Research Institute of Arctic Geology, 95: 104-122 (in Russian).
Ravich M G. 1960. Preliminary results of geological survey of the Bunger Hills oasis area. Proceedings of the Soviet Antarctic Expedition, 9: 171-184 (in Russian).
Ravich M G, Solovyev D S. 1966. Geological map of the Bunger Oasis, 1:100,000 scale//Bakaev V G, Tolstikov E I (eds). Atlas of Antarctica, Vol. I. Moscow: Central Board of Geodesy and Cartography, 166-167 (in Russian).
Shary P A, Sharaya L S, Mitusov A V. 2002. Fundamental quantitative methods of land surface analysis. Geoderma, 107(1/2): 1-32, doi: 10.1016/S0016-7061(01)00136-7.
Sheraton J W, Tingey R J. 1994. Bedrock geology of the Bunger Hills–Denman Glacier region, 1:250,000 scale map. Canberra: Australian Geological Survey Organisation.
Sheraton J W, Tingey R J, Oliver R L, et al. 1995. Geology of the Bunger

Hills–Denman Glacier region, East Antarctica. Australian Geological Survey Organisation Bulletin, 244: 1-124, doi: 10.26186/5c638cd2a20a0.

Shumskiy P A. 1957. Glaciological and geomorphological reconnaissance in the Antarctic in 1956. J Glaciol, 3(21): 54-61, doi: 10.3189/s0022143000024758.

Simonov I A. 1971. Oases of East Antarctica. Leningrad: Hydrometeoizdat (in Russian).

Sokratova I N. 2010. Antarctic oases: history and results of investigations. St. Petersburg: Arctic and Antarctic Research Institute (in Russian).

Trevisani S, Guth P L. 2024. Terrain analysis according to multiscale surface roughness in the Taklimakan Desert. Land, 13(11): 1843, doi: 10.3390/land13111843.

Trevisani S, Teza G, Guth P L. 2023. Hacking the topographic ruggedness index. Geomorphology, 439: 108838, doi: 10.1016/j.geomorph.2023.108838.

Tucker N M, Hand M, Clark C. 2020. The Bunger Hills: 60 years of geological and geophysical research. Antarct Sci, 32(2): 85-106, doi: 10.1017/s0954102019000403.

Verkulich S R. 1995. History of the development of the natural environment of the Bunger Oasis (East Antarctica) at the end of the Late Pleistocene and Holocene, Ph. D. thesis. St. Petersburg: St. Petersburg University (in Russian).

Wilson J P, Gallant J C (eds). 2000. Terrain analysis: principles and applications. New York: Wiley.

Wisniewski E. 1983. Bunger Oasis: the largest ice-free area in the Antarctic. Terra, 95(3): 178-187.